

The Effect of Wing Corrugations on the Aerodynamic Performance of Low-Reynolds Number Flapping Flight

S. Premachandran and M. Giacobello

Air Vehicles Division, Defence Science and Technology Organisation
 506 Lorimer St, Fishermans Bend VIC 3207, Australia

Abstract

The effect of wing corrugations on the aerodynamic performance of low Reynolds number hovering flight is investigated using two-dimensional Computational Fluid Dynamics. Corrugated sections with peaks that follow the contours of NACA sections are compared with the corresponding NACA airfoils, a flat plate of the same wall thickness as the corrugated sections, and a 1:4 ellipse. Simplified kinematics comprising combined heaving and pitching motions were simulated, and it was found that the thinner airfoil-type sections produced more lift than the thicker sections. The corrugated sections were found to perform similarly regardless of the size of the corrugated peaks and the orientation of the leading edge. The net vertical force in all of the corrugated cases was approximately the same as for the flat plate, indicating that wing corrugations produce no direct benefit in the generation of net vertical force for wings operating with hovering kinematics.

Introduction

Many insects display highly manoeuvrable flight, and they are able to generate high lift at very low Reynolds numbers (Re). Interest in these capabilities has inspired considerable research into the aerodynamic mechanisms of insect gliding and flapping-flight.

Insect wings, unlike traditional airfoils, have sharply corrugated cross-sections. These corrugations increase spanwise stiffness with little weight penalty. The aerodynamic effect of corrugations in the flapping-flight regime remains a topic for investigation, while their effect in gliding flight has been the focus of a number of earlier studies [2-5,7].

For steady gliding flight at suitably low Re , past experimental and numerical studies have indicated that the wing corrugations can enhance performance. Okamoto *et al.* [5] conducted experiments on two-dimensional (2D) wing models in a steady crossflow and found that a corrugated wing produced a higher maximum lift than a flat plate, when the leading edge was downward facing; while an upward-facing leading edge produced less lift. Kesel [2] extracted three representative wing sections from the dragonfly *Aeshna cyanea*, with downward-facing, upward-facing, and horizontal leading edges and compared these to the corresponding smoothly contoured sections derived by connecting the local corrugation extrema, and to a flat plate. The sections with downward- and upward-facing leading edges produced higher lift than the flat plate, while the section with a horizontal leading edge produced lift comparable to that of a flat plate. The corresponding profiled section produced lift similar to that of a flat plate. The numerical study of Vargas *et al.* [7] considered the sections used by Kesel and also found that a corrugated airfoil produced higher lift than a profiled section, while giving comparable drag.

In flapping flight, where the insect is able to generate the most lift, a different aerodynamic mechanism is utilised. Studies have

shown that the flapping motion creates downward-convecting vortex rings, inducing a net upward force. For insects that flap along an inclined stroke plane, the wing kinematics follow a paddling-type motion. The vertical force is generated primarily on the downstroke, when the wing is translating at a large angle relative to the flow (often around 35–40° [8]). This means that the lift force in the classical sense (the force perpendicular to the oncoming flow) is no longer the dominant component. In fact the generation of a net vertical force is more of a drag-based mechanism. To-date, there has been no comparison of the performance of corrugated and smooth wings in the flapping-flight regime.

The wing motion of insects such as hawkmoths, locusts, and dragonflies is a superposition of a heaving motion and a pitching motion. In this study, the 2D, generic kinematics suggested by Wang [9] for a hovering dragonfly illustrated in Figure 1 are used. This comprises a heaving motion along an inclined stroke plane, $\beta = 60^\circ$, given by

$$A(t) = A_o / 2 [\cos(2\pi t / T) + 1], \quad (1)$$

and a pitching motion, given by

$$\alpha(t) = \pi / 4 - \pi / 4 \sin(2\pi t / T), \quad (2)$$

where A is the distance travelled by a point at the centre of the wing chord along a line inclined at an angle β from the x axis and α is the instantaneous pitch angle of the wing. A_o is the total linear excursion of the wing, c is the wing chord, and T is the wingbeat period. Re is here based on the chord length and the maximum translational speed of the wing ($U_o = A_o\pi/T$). For all simulations, $A_o/c = 2.5$, $T = 0.025$ s, $c = 1 \times 10^{-2}$ m, and $Re = 157$. These length and velocity scales are also used in computing the force coefficients. The force coefficients resolved along the x and y axes are denoted by C_H and C_V , respectively.

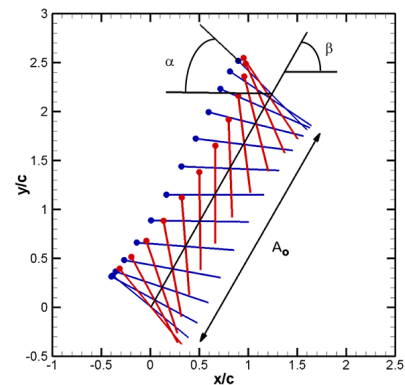


Figure 1. Definition of wing kinematics. Chord line shown at intervals of 0.047, with blue denoting the downstroke and red the upstroke.

The sections considered are illustrated in Figure 2 and comprise (a) a flat plate, (b) 6% and 12%-thickness, symmetric NACA airfoils (NACA0006 and NACA0012), and (c and d) saw-tooth

corrugated sections that have five corrugation peaks that follow the contours of the NACA sections. Because the corrugation peaks follow the contour of the filled sections, the effective camber and thicknesses are the same, and the results may be directly compared. The number of peaks was selected based on the wing-section profiles presented in Kesel [2], which indicate that 5–7 peaks are typical of the *Aeshna cyanea* wings. Sections with (c) upward-facing and (d) downward-facing leading- and trailing-edge sections are considered. The leading edges are inclined at 9° and 18° to the chord-line for the NACA0006-based and NACA0012-based sections respectively. The corrugated and flat-plate sections have blunt leading edges and a thickness of $1 \times 10^{-3} c$. To validate the numerical approach, a 1:4 ellipse considered by Wang [9] is also evaluated (not shown in Figure 2).



Figure 2. Wing sections under investigation.

The instantaneous and time-averaged vertical forces for each section are compared and related to visualisations of the flow structures. Conclusions are drawn about the relative performance of the various wing sections in the flapping-flight regime.

Numerical Method and Validation

The commercial finite-volume solver Fluent 12.1 was used to solve the unsteady incompressible Navier–Stokes equations using the pressure-based solver and the SIMPLE algorithm to achieve velocity–pressure coupling. The wing motion was prescribed using the dynamic meshing feature, which, in the current implementation, is limited to first-order temporal accuracy. Spatial discretisation was second-order accurate.

The computational domain was discretised using a structured layer of quadrilateral cells adjacent to the wing, and triangular cells extended from the edge of the structured layer to the far-field boundary, as shown in Figure 3. The outer boundary of the computational domain comprised a circle of diameter 80 times the chord length, centred at the centre of the wing. Figure 3 presents two views of the near-field grid using the flat plate section as an example. At the wing surface, a no-slip wall boundary condition was enforced, while at the far-field boundary a zero-gradient outflow boundary condition was used. All simulations were initialised with a zero-velocity field and run until the instantaneous force coefficients reached a periodic state (roughly ten flapping periods, or $t/T = 10$).

The adequacy of the temporal and spatial resolution was assessed for the flat plate by decreasing the time step and increasing the grid resolution until the average horizontal- and vertical-force coefficients (\bar{C}_H and \bar{C}_V) changed by less than 1%. Figure 4 compares the time history of C_V with the results of Wang [9], Gao & Lu [1], and Sudhakar & Vengadesan [6]. The result of the current study is within the scatter of these earlier results.

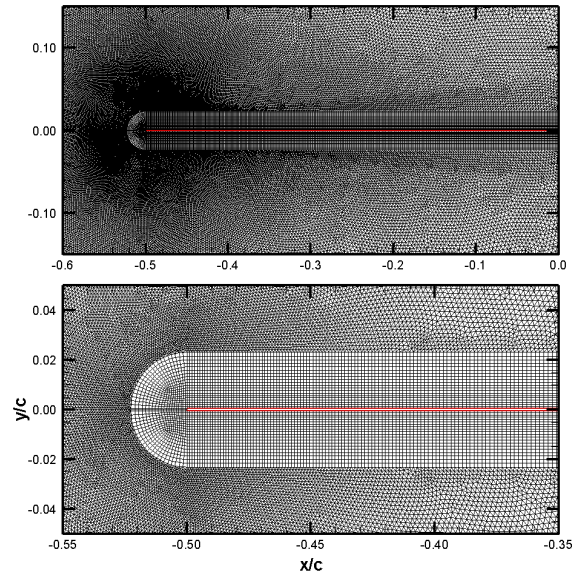


Figure 3. Near field grid for a flat-plate wing section.

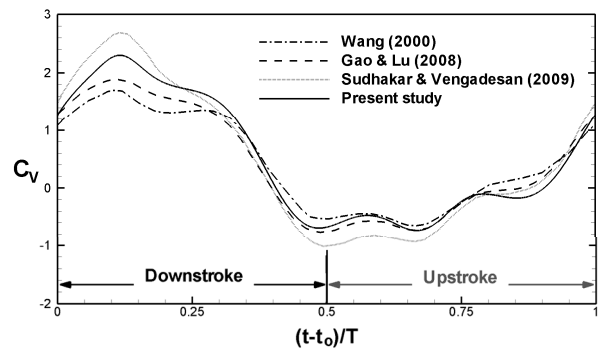


Figure 4. Comparison with earlier studies of the C_V time history for a 1:4 ellipse.

Results and Discussion

Instantaneous Forces and Flowfields

The vertical-force coefficient over two flapping cycles is shown in Figure 5. Figure 5a compares the filled airfoil with the two corrugated sections (corresponding to the profiles show in Figure 2b–d) for the NACA0006 profile. The results for the NACA0012-based corrugated sections are omitted because the trends were found to be very similar. For the NACA0006-based geometries, the peak-to-peak amplitudes are slightly larger for the corrugated sections than for the smooth section, and the section with a downward-facing leading edge has a slightly higher peak C_V than that with an upward-facing leading edge. These variations in peak-to-peak amplitude may have practical design implications on the strength (and therefore thickness) requirements of the wing structure.

Figure 5b compares the results for the smooth profiles (the flat plate, the NACA airfoils, and the ellipse). For the thin wing sections (*i.e.*, all of the geometries considered, except for the 1:4 ellipse), the time histories of vertical-force generation are quite similar. The main differences are in the peak negative and positive force magnitudes. Decreasing the thickness of the wing section results in larger peak-to-peak C_V fluctuations. Figure 6 presents the pressure difference between the lower and upper surface, ΔC_p , at the point of maximum C_V ($t/T=11.11$). The increase in peak lift is shown to be a result of a net increase in ΔC_p . This difference is more pronounced near the leading edge, where the geometries are the most different.

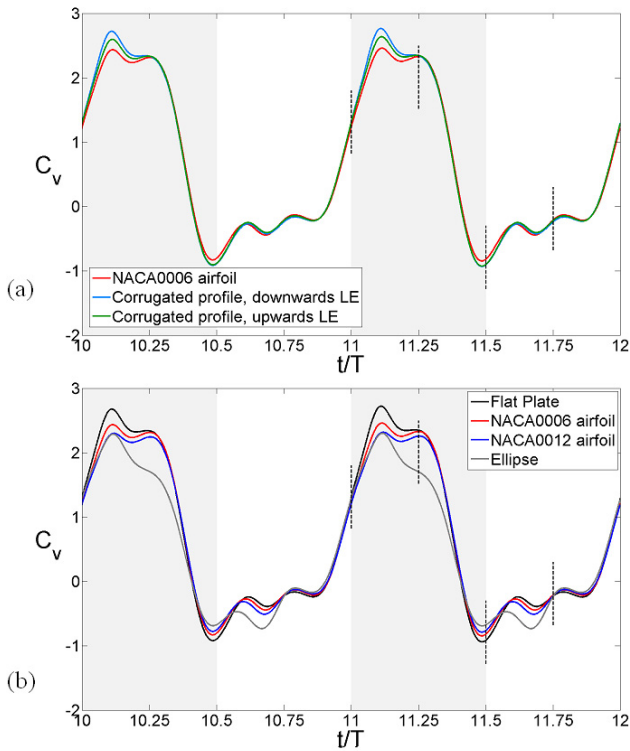


Figure 5. Instantaneous vertical-force coefficients across two periods for (a) the NACA0006-based sections and (b) the smooth airfoils. Shaded regions correspond to the downstroke, and dashed lines correspond to the times shown in Figure 7.

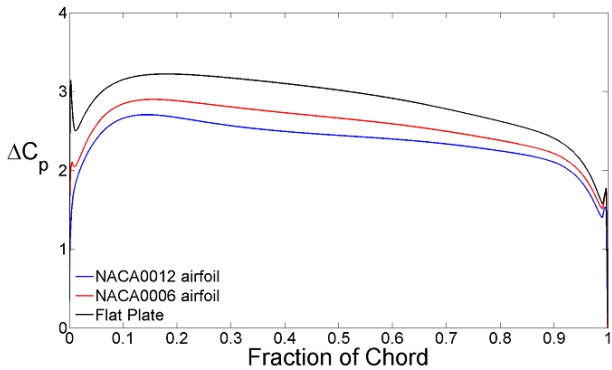


Figure 6. Pressure difference between the lower and upper surface, ΔC_p along the chord at $t/T=11.11$.

The general lift mechanism is illustrated in Figure 7 for the flat plate, the NACA0006 airfoil, and the NACA0006-based corrugated section with a downward-facing leading edge. The other geometries exhibited the same behaviour. Similar to the observations of Wang [9] for the 1:4 ellipse, Figure 7 shows that vortices of opposite rotation are generated at the leading and trailing edge during the downstroke, which then combine into a dipole before detaching from the wing during the rotation at the bottom of the stroke. This dipole is convected downward, inducing a net upward force on the wing. There are slight differences across the geometries in the immediate vicinity of the wing sections, but the flow structures farther away are very similar, consistent with the similarity in the time histories of Figure 5. This agrees with the observations of Kim *et al.* [4] for wing sections in steady crossflow, where the wider flowfield was also found to be unaffected by the wing geometry. It is interesting to note that although several previous studies on airfoils in gliding flight showed that corrugations delay the onset

of stall (for example, Murphy & Hui [3] and Kesel [2]), here no major differences in the flowfield were observed between the flat plate and the corrugated sections at any point in the flapping cycle.

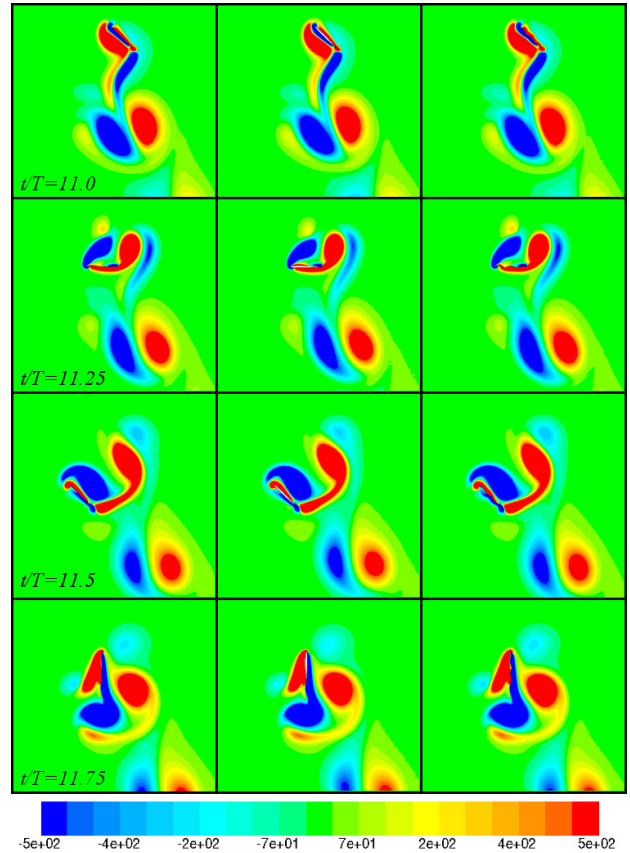


Figure 7. Contours of vorticity at different times for (left) the flat plate, (middle) the NACA0006 airfoil and (right) the NACA0006-based, corrugated airfoil with a downward-facing leading edge.

Figure 8 shows the distribution of the pressure coefficient at $t/T = 11.25$ for the corrugated sections and the flat plate. The corrugations have a more significant effect on the lower surface of the airfoil (the surface with positive pressure). At $t/T = 11.25$ the wing is halfway through its downstroke, so the lower surface faces the oncoming flow (the windward side). The upper surface is exposed to a separated, recirculating wake and the surface pressure distribution is less affected by the geometry. Over the lower surface, for the two sections with downward-facing leading edges, there are two chordwise stations where the pressure changes sharply. These correspond to the locations of the downward-pointing corrugation peaks (see Figure 2c), which face into the wind. The pressure distribution is fairly smooth across the upward-facing peaks. The magnitude of the discontinuous pressure peaks is roughly twice as large for the NACA0012-based section as for the NACA0006-based section. The results for the upward-facing leading-edge section show similar trends: sharp discontinuities on the windward surface, where the corrugated peaks are facing into the flow, and relatively little effect over the upper surface, and where the corrugations are facing away from the flow.

Average Forces

In order to draw conclusions about the overall performance of the different sections, the net vertical force over the cycle must be considered, as it is the net vertical force that enables an insect to sustain hovering. The time-averaged vertical-force coefficients (\bar{C}_v) are shown in Figure 9.

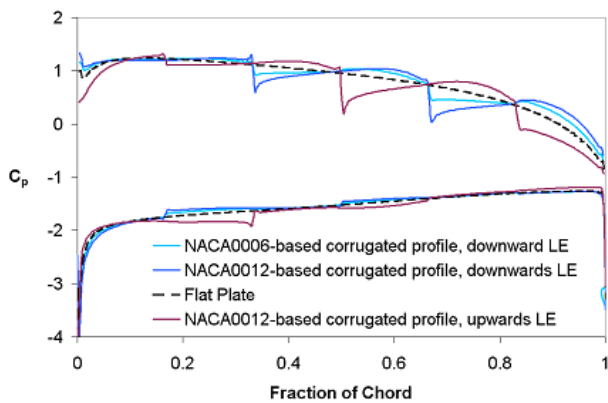


Figure 8. Pressure coefficient over upper and lower wing surfaces at $t/T = 11.25$ for several corrugated wing sections and a flat plate.

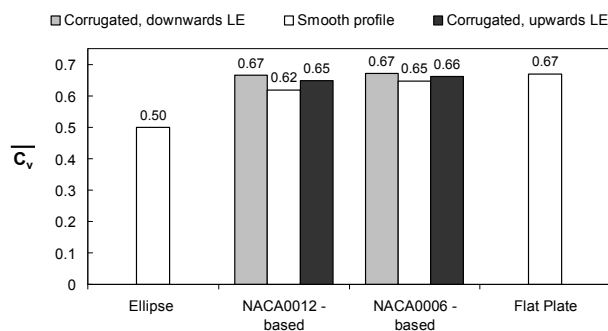


Figure 9. Time-averaged C_T for each wing section.

The smooth profiles (the ellipse, airfoils, and flat plate) are arranged from left to right by decreasing thickness (maximum profile thickness of 25% of chord for the ellipse, down to 0.1% for the flat plate). The thinner sections perform better than thicker sections in terms of net vertical-force generation, consistent with the observations made by Wang [10] for elliptical sections. However Figure 5 shows that the thinner sections also have greater peak-to-peak force fluctuations, so they may not necessarily be the most suitable in a practical design context.

The corrugated wing sections were found to perform slightly better than their smooth-airfoil counterparts. Based on the flowfield visualisations, it seems more likely that this is due to the smaller wall thickness at the leading and trailing edges than to the shape of the corrugations. It is interesting to note that the performance of the flat plate is essentially the same as for the corrugated profiles. This suggests that the corrugations do not have a significant, direct effect on the vertical force. However, in a biological system or in a micro-aerial-vehicle application, they may indirectly affect the aerodynamic performance by controlling the wing stiffness and therefore its deformation under load. The second moment of area about the chord axis is four orders of magnitude larger for the NACA0012-based corrugated section than for the flat plate, so the wing sections will deform differently when subject to flapping loads.

The effect of the orientation of the corrugations is less pronounced; the difference is approximately 2% for both the NACA0006- and NACA0012-based profiles, which is practically insignificant. However it is noted that for both groups of corrugated sections the downward-facing leading edge is shown to produce slightly more net vertical force than the upward-facing leading edge. Okamoto *et al.* [5] found that a downward-facing leading edge produced higher lift in gliding flight, although they reported a more significant difference (of the order of $\Delta C_L = 0.1$).

Overall the individual values of \bar{C}_v (excluding the ellipse) vary by less than 6% from the group mean, indicating that the effect of wing-section shape on net vertical force is relatively minor. For this sort of hovering kinematics, the aerodynamic mechanism generating this vertical force is more akin to classical drag than lift [8]. For example at $t/T = 11.25$, when the wing is halfway through the downstroke, approximately 75% of the vertical force comes from the drag force (the force parallel to the relative wind). In steady flow at high angles of attack, the main component of the drag force is the pressure drag. Several studies on corrugated wings in steady crossflow [3, 7] have shown that trapped vortices form in the valleys of the corrugations, causing the outer streamlines to flow smoothly over the wing. This gives the wing an 'effective' shape similar to that of a filled airfoil. As a result the drag tends to be similar for the corrugated and filled airfoils in the post-stall region [3] in steady flow. A similar effect appears to occur in the flapping regime, causing the net drag (and by extension, the vertical force) to be similar across the geometries.

Conclusions

For the 2D flapping-flight kinematics simulated in this study, it was found that thinner wings tend to generate greater net vertical forces and slightly higher peak-to-peak force fluctuations. For corrugated profiles, geometries with downward-facing leading edges produced slightly more lift, but the effect is small and could be considered insignificant. The net vertical force of the corrugated wing sections were approximately the same as for the flat plate. The main effect of the corrugations is to alter the pressure distribution on the windward side of the wing surface.

References

- [1] Gao, T. & Lu, X., Insect Normal Hovering in Ground Effect, *Phys. Fluids*, **20**, 2008, 087101.
- [2] Kesel, A., Aerodynamic Characteristics of Dragonfly Wing Sections Compared with Technical Aerofoils. *J. Exp. Biology*, **203**(20), 2000, 3125-3135.
- [3] Murphy, J.T. & Hu, H., An Experimental Study of a Bio-inspired Corrugated Airfoil for Micro Air Vehicle Applications. *Exp. Fluids*, **49**(2), 2010, 531-546.
- [4] Kim, W.-K., Ko, J.H., Park, H.C. & Byun, D., Effects of Corrugation of the Dragonfly Wing on Gliding Performance. *J. Theor. Biol.*, **260**(4), 2009, 523-530.
- [5] Okamoto, M., Yasuda, K. & Azuma, A., Aerodynamic Characteristics of the Wings and Body of a Dragonfly. *J. Exp. Biology*, **199**(2), 1996, 281-294.
- [6] Sudhakar, Y. & Vengadesan, S., Flight Force Production by Flapping Insect Wings in Inclined Stroke Plane Kinematics. *Comp. Fluids*, **39**(4), 2010, 283-295.
- [7] Vargas, A., Mittal, R. & Dong, H. A Computational Study of the Aerodynamic Performance of a Dragonfly Wing Section in Gliding Flight. *Bioinsp. Biomim.*, **3**(2), 2008.
- [8] Wang, Z.J., The Role of Drag in Insect Hovering. *J. Exp. Biology*, **207**(23), 2004, 4147-4155.
- [9] Wang, Z.J., Two Dimensional Mechanism for Insect Hovering, *Phys. Rev. Lett.*, **85** (10), 2000, 2216-2219.
- [10] Wang, Z.J., Vortex Shedding and Frequency Selection in Flapping Flight. *J. Fluid. Mech.*, **410**, 2000, 323-341.